

CrystEngComm

Accepted Manuscript



This is an *Accepted Manuscript*, which has been through the Royal Society of Chemistry peer review process and has been accepted for publication.

Accepted Manuscripts are published online shortly after acceptance, before technical editing, formatting and proof reading. Using this free service, authors can make their results available to the community, in citable form, before we publish the edited article. We will replace this *Accepted Manuscript* with the edited and formatted *Advance Article* as soon as it is available.

You can find more information about *Accepted Manuscripts* in the [Information for Authors](#).

Please note that technical editing may introduce minor changes to the text and/or graphics, which may alter content. The journal's standard [Terms & Conditions](#) and the [Ethical guidelines](#) still apply. In no event shall the Royal Society of Chemistry be held responsible for any errors or omissions in this *Accepted Manuscript* or any consequences arising from the use of any information it contains.

Fabrication and photoluminescence properties of TiO₂:Eu³⁺ microspheres with tunable structure from solid to core-shell

Ming Yan^b, Haifeng Zou^a, Huan Zhao^a, Yanhua Song^a, Keyan Zheng^a, Ye Sheng^{a*}, Guanjun Wang^{b*},
Qisheng Huo^c

^a College of Chemistry, Jilin University, Changchun 130012, PR China

^b Spine Center of the First Hospital of Jilin University, Changchun 130021, PR China

^c State Key Laboratory of Inorganic Synthesis and Preparative Chemistry, College of Chemistry, Jilin University, Changchun 130012, PR China

Abstract: Monodisperse solid and core-shell structured TiO₂:Eu³⁺ microspheres have been successfully prepared by a facile one-step hydrothermal method using polyethylene glycol (PEG, MW 20000) as the soft template, titanium tetrabutoxide (TBOT) as the titanium source, and ethanol as the solvent. The XRD patterns show that the direct hydrothermal synthesized products are anatase titanium dioxides. TEM and SEM observations indicate that the amount of ethanol plays an important role in the formation of TiO₂:Eu³⁺ microspheres. Solid TiO₂:Eu³⁺ microspheres were formed under small amounts of ethanol, while core-shell structured ones were formed under large amounts of ethanol. Possible growth mechanisms of both the solid and core-shell structured TiO₂:Eu³⁺ microspheres were also proposed in this paper. In addition, without any further calcination, the direct hydrothermal synthesized solid and core-shell structured TiO₂:Eu³⁺ microspheres show strong red emission corresponding to the ⁵D₀→⁷F₂ transition of the Eu³⁺ ions under ultraviolet excitation. However, the luminescence intensity of the solid microspheres is much higher than that of the core-shell structured TiO₂:Eu³⁺ microspheres, which might due to the fewer defects and much more effectively doping of Eu³⁺ ions in the solid

microspheres.

Keywords: solid, core-shell, TiO₂, Eu³⁺, microspheres

1. Introduction

In recent years, fabrication of three-dimensional (3D) microspheres including solid and core-shell structure has attracted considerable attention due to their excellent properties and potential applications¹⁻³. Thus, great efforts have been dedicated to explore new approaches for the fabrication of microspheres in different systems. Among various synthesis methods, the hydro/solvothermal process has been proved to be one of the most effective and convenient synthesis techniques in obtaining microspheres owing to its mild reaction conditions, tunable reaction parameters, and large-scale production capability⁴⁻⁶. However, it's well known that the reaction parameters, such as reaction time and temperature, pH value of the precursor solution, and surfactants and solvents used, affect the crystal growth behavior directly^{7,8}. Therefore, it is important to clarify the effect of reaction conditions on the sample shapes and discuss the formation mechanisms of different morphologies, which will guide the design and preparation of new inorganic functional materials⁹.

Due to its chemical stability, easy synthesis, low cost, non-toxic, and non-hygroscopic performance, titania (TiO₂) is suggested to be a promising host material for the luminescence of various rare earth ions¹⁰⁻¹². Therefore, many efforts have been devoted to explore various morphologies of TiO₂-based phosphors, such as nanorods¹³, nanotubes¹⁴, nanowires¹⁵, nanorings¹⁶, nanoplates¹⁷, microspheres^{18, 19}, core-shell structure²⁰, and hollow spheres²¹, etc. However, to the best of our knowledge, there have been few reports on the synthesis and their corresponding luminescence of uniform, well-dispersed submicron-scaled Eu-doped TiO₂ spheres with tunable structure from solid to

core-shell.

The synthesis of core-shell structured TiO₂ microspheres via the Ostwald ripening process reported by Yuming Cui et al.²², Zeng's group²³, and Hexing Li et al.²⁴ has attracted significant scientific interest. The interest is motivated by their adjustable morphology, size, and interior structure. However, in these literatures, the effect of amount of solvent on the morphology of the products hasn't been mentioned. This work, for the first time, reports the synthesis of TiO₂:Eu³⁺ spheres with tunable structure from solid to core-shell by simply tuning the amount of ethanol. The possible formation mechanisms were suggested. In addition, the shell and core size of the core-shell structured TiO₂:Eu³⁺ microspheres can be also easily tuned by controlling the hydrothermal time through the Ostwald ripening process. Without any further calcination, the direct hydrothermal synthesized solid and core-shell structured spheres show strong red emission under ultraviolet excitation, but their luminescence intensity is different. The possible reason was discussed.

2. Experimental Section

2.1. Materials

Eu(NO₃)₃ aqueous solution was obtained by dissolving Eu₂O₃ (99.99%) in dilute HNO₃ solution under heating with agitation. All other chemical reagents were of analytical grade and used without further purification.

2.2. Synthesis

In a typical experimental procedure, 2.0 g of PEG was dissolved in 18 mL of ethanol under heating. After the solution being cooled to room temperature, 1.2 mL of HCl, 2.4 mL of glacial acetic acid, and specific amount of Eu(NO₃)₃ were added and stirred for 5 min. 1.7 mL of tetrabutyl titanate was dropped into the above mixture solution and then 1.0 g of urea (CO(NH₂)₂) was added and stirred for

10 min again. Finally, the mixture was transferred into a Teflon-lined stainless steel autoclave (50 mL capacity). The autoclave was heated and held at 180 °C for 12 h and then allowed to cool to ambient temperature naturally. After the reaction, the products of the hydrothermal reaction were collected, washed with distilled water and ethanol for four times alternately, and dried in the air for 12 h at 60 °C. The resulting sample was labeled as S1. Other conditions were constant, when the amount of ethanol was added to 30 mL, resulting sample was labeled as S2. Parallel experiments were carried out to examine various synthetic parameters.

2.3. Characterization

X-ray diffraction (XRD) experiments were carried out using a XRD-6000 X-ray diffractometer (Shimadzu) with Cu K α radiation ($\lambda=0.154056$ nm). The size and morphology of the samples were inspected using a field emission scanning electron microscope equipped with an energy-dispersive spectrometer (EDS) (FE-SEM, S-4800, Hitachi, Japan). The transmission electron microscopy (TEM) images were obtained by a FEI Tecnai G² S-Twin transmission electron microscope with a field emission gun operating at 200 kV. The photoluminescence spectra (PL) were observed using a Jobin Yvon FluoroMax-4 equipped with a 150 W xenon lamp as the excitation source. All the measurements were performed at room temperature. The X-ray photoelectron spectra (XPS) were taken on a VG ESALAB 250 electron energy spectrometer using Mg K α (1253.6 eV) as the X-ray excitation source.

3. Results and discussion

Figure 1 (A) shows the X-ray diffraction (XRD) patterns of TiO₂:Eu³⁺ solid microspheres (S1) and core-shell microspheres (S2), which indicate that both S1 and S2 are all the anatase phases of titania. The strong and sharp diffraction peaks indicate the good crystallinity of the as-synthesized products by the direct hydrothermal process without further sintering. The anatase phase with good crystallinity is

beneficial to the luminescence of Eu^{3+} ions²⁵. Careful view shows that the position of XRD peaks, especially the prominent (101) peaks of S1 and S2 are shifted toward much higher 2θ value compared with the standard XRD pattern, as shown in Figure 1(B). This is attributed to the large mismatch in ionic radius between Eu^{3+} and Ti^{4+} . For hetero-valence ion doping, the variations of crystal lattice are complex due to the requirement of extra vacancy or interstitial ions to compensate charge.²⁶ Therefore, we can't infer the position of Eu^{3+} doping, but the notable angle shift of S1 and S2 compared with the standard XRD pattern indicate that Eu^{3+} ions have been doped in the TiO_2 crystal lattice. In addition, the peaks of S1 are shifted toward much higher 2θ value than those of S2, which also indicate that Eu^{3+} ions in S1 are doped much more effectively than Eu^{3+} ions in S2.

In order to investigate the element composition, the as-prepared samples were analysed by Energy-dispersive spectrometry (EDS) and the EDS of S1 was shown in Figure 2 (the EDS of S2 is similar to that of S1 and it was not shown here). The EDS result confirms the presence of titanium (Ti), oxygen (O), and europium (Eu) elements in $\text{TiO}_2:\text{Eu}^{3+}$ solid microspheres and core-shell microspheres. No other peaks of impurity elements were detected, which gives further support for the XRD analysis above.

The chemical components of as-synthesized Eu-doped TiO_2 samples were further analyzed by X-ray photoelectron spectroscopy. A typical XPS survey scan for S1 and S2 (solid and core-shell $\text{TiO}_2:\text{Eu}^{3+}$) over a large energy range is presented in Fig. 3A, it can be seen that there are Eu 3d, Eu 4d, Ti 2p, O 1s, and C 1s XPS lines, among them C 1s spectrum is due to the contamination of CO_2 in air and carbon on the substrate, while the existences of Eu 3d, Eu 4d, Ti 2p, O 1s further confirm the EDS results. Figure 3B shows the Ti 2p_{1/2} and Ti 2p_{3/2} spectra of S1 and S2. The Ti 2p_{3/2} peaks of S1 and S2 are all shifted from 459.4 eV in pure TiO_2 ²⁷ to 458.9 eV in S1 and S2. This shifting represents an

intermediate oxidation state of Ti from tetra- to trivalent²⁷ due to the doping of Eu^{3+} . Figure 3C shows O 1s spectra of S1 and S2. As reported in the literature^{28,29}, the O 1s binding energy of pure TiO_2 is ~ 530.0 eV. However, for O 1s spectra of S1 and S2, an intense peak was found at BE (530.2 eV) and a shoulder at BE (532.0 eV). The Eu $3d_{5/2}$ and Eu $4d_{5/2}$ peak of S1 is found at 1135.4 eV and 136.7 eV respectively, while the Eu $3d_{5/2}$ peak Eu $4d_{5/2}$ peak of S2 is at 1134.7 eV and 137.1 eV, respectively. The data available in the literatures for Eu_2O_3 are the values 1134.2 and 135.0 eV for the Eu $3d_{5/2}$ and Eu $4d_{5/2}$ peaks, respectively^{30, 31}. These different binding energies correspond to different chemical environments³², which further indicate that the crystal environments of Eu^{3+} are different for the solid and the core-shell microspheres, and Eu^{3+} ions have been effectively doped in S1 and S2, rather than simply being mixed.

The morphology and structure of the products were examined by scanning electron microscope (SEM) and transmission electron microscope (TEM). Figure 4a shows a panoramic SEM image of the as-prepared S1. From Figure 4a, it can be seen that S1 mainly contains uniform spheres with an average diameter of about 2.0 μm . A high-magnification SEM image reveals that the surface of the microspheres is smooth (Figure 4b). TEM images of S1 (Figure 4c and 4d) clearly show that the sample consists of uniform, smooth, monodisperse, and solid microspheres with diameters of about ~ 2.0 μm . In contrast, S2 is composed of uniform spheres with a mean diameter of ~ 2.4 μm and there appear two or three microspheres attached together (Figure 5a). More careful examination of the high-magnification SEM image (Figure 5b) verifies that the surface of S2 is rough and the core-shell structure can be seen more clearly from the SEM image of the cracked microsphere. As shown in Figure 5c and 5d, the dark center and pale edge of the microspheres further prove the core-shell nature of S2. The shell thickness of the spheres is about 50 nm, which is identical to the SEM observations.

The results reveal that the amount of ethanol plays a critical role in the formation of $\text{TiO}_2:\text{Eu}^{3+}$ microspheres.

To inspect the role of the amount of ethanol, different amount of ethanol was used while other reaction parameters remained unchanged. Figure 6 shows the SEM images of solvothermal samples obtained when different amount of ethanol was added. From Figure 6, it can be seen that the obtained microspheres are solid and their surfaces are smooth under small amounts of ethanol (15 mL, 18 mL, and 21 mL). However, with the increase of the amount of ethanol to 22 mL, the surface of the microspheres tends to become rough. Upon further increasing the amount of ethanol to 24 mL, rough and core-shell structured microspheres are formed. When the amount of ethanol reached 30 mL, obvious core-shell structured and uniform microspheres can be clearly observed. In addition, the core-shell structured microspheres are a little larger than the solid microspheres.

To shed light on the formation of the two kinds of microspheres and to enrich the crystal growth mechanism of TiO_2 microspheres, time-dependent experiments of S1 and S2 were performed while the other reaction parameters remained unchanged. Interestingly, we find that there is a large difference between the two kinds of microspheres. With the increase of the hydrothermal reaction time, the morphology of the solid microspheres is not changed, namely, they are still solid microspheres. However, the hydrothermal time has a great influence on the core-shell structured microspheres. With a short hydrothermal reaction time (45 min and 90 min, Figure 7a, b), there is no gap between the core and shell. When the hydrothermal reaction time increased to 12 h, a small gap appeared. Furthermore, as shown in Figure 7c-f, the core becomes smaller while the shell gets thicker, namely the gap turns bigger with increasing the hydrothermal reaction time (12 h, 18 h, 4 days, and 6 days). On the basis of these images, it is speculated that the core-shell structured microspheres undergo an Ostwald ripening

process when the hydrothermal time is prolonged as reported by Yuming Cui²². This is a sophisticated process of the Ostwald ripening mechanism; during this process, the inner titania crystallites of the core, which have a higher surface energy and a smaller diameter, would dissolve and transfer to the outer space in the oxide shells and redeposit and recrystallize on the better crystallized TiO₂ nanoparticles of the shell.

Summing up the above results and discussions, most plausible formation mechanisms of the solid and core-shell structured microspheres are proposed and schematically illustrated in Figure 8. First, as the literatures^{22, 33, 34} reported, the aggregated acid-stabilized Ti(OBu)_nL_{4-n}-PEG-urea globules are formed by the weak coordination interaction and the hydrogen bonding. For the system of the small amount of solvent ethanol, the concentration of PEG is higher and the PEG chains in the globules are relatively denser than that of large amounts of ethanol. Second, Ti(OBu)₄ is gradually hydrolyzed into TiO₂ under the action of the soft templates Ti(OBu)_nL_{4-n}-PEG-urea globules. For the system of S1, the high viscosity and dense chains make the formed TiO₂ difficult to move and solid microspheres are gradually formed. However, for the system of S2, more solvent ethanol make the pressure of the system bigger; the existing pressure and temperature gradient along the outer surface to the inner of Ti(OBu)_nL_{4-n}-PEG-urea globules make the formation of TiO₂ nanoparticles layers on the exterior of the globules. The relatively low viscosity and loose chains allow the formed TiO₂ move to the exterior of the globules. And just as the literature²² suggested, the hydrothermal decomposition of the urea molecules brings tiny CO₂ gas bubbles in the globules, and the tiny gas bubbles are confined in the globule by the surface-covered TiO₂ nanoparticles. Therefore, the core-shell structured TiO₂ microspheres were formed by the reaction of acid-stabilized Ti(OBu)_nL_{4-n} with NH₃·H₂O released from the hydrothermal decomposition of urea in the confined interior of the microspheres during the

hydrothermal process.

Figure 9 shows the emission and excitation (inset) spectra of the obtained S1 and S2, both of them have similar photoluminescent (PL) properties. The excitation spectrum, monitored with 612 nm emission of Eu^{3+} ($^5\text{D}_0 \rightarrow ^7\text{F}_2$), consists of the characteristic excitation lines of Eu^{3+} within its $4f_6$ configuration from 300 to 500 nm. The peaks at 361, 384, 394, 415, and 464 nm can be clearly observed which correspond to $^7\text{F}_0 \rightarrow ^5\text{D}_4$, $^7\text{F}_0 \rightarrow ^5\text{G}_2$, $^7\text{F}_0 \rightarrow ^5\text{L}_6$, $^7\text{F}_0 \rightarrow ^5\text{D}_3$, and $^7\text{F}_0 \rightarrow ^5\text{D}_2$ transitions of Eu^{3+} , respectively. Upon excitation at 394 nm, the emission spectra of both the solid and core-shell $\text{TiO}_2:2\% \text{Eu}^{3+}$ microspheres are composed of a group of lines peaking at about 578, 590, 612, 651, and 696 nm. They come from the $^5\text{D}_0 \rightarrow ^7\text{F}_j$ ($j = 0, 1, 2, 3, 4$) transitions of the Eu^{3+} ions. The $^5\text{D}_0 \rightarrow ^7\text{F}_1$ transition at 590 nm was the parity-allowed magnetic dipole transition ($\Delta J = 1$), and the $^5\text{D}_0 \rightarrow ^7\text{F}_2$ transition at 612 nm was the electric dipole transition ($\Delta J = 2$).³⁵ It is well-known that the relative intensity of the $^5\text{D}_0 \rightarrow ^7\text{F}_1$ and $^5\text{D}_0 \rightarrow ^7\text{F}_2$ transition is also determined by the symmetry of the crystal sites of the Eu^{3+} ions. If Eu^{3+} ions has a site with inversion symmetry, the $^5\text{D}_0 \rightarrow ^7\text{F}_1$ transition dominates; while if Eu^{3+} ion holds a site without inversion symmetry, the $^5\text{D}_0 \rightarrow ^7\text{F}_2$ transition predominates.³⁶ In the case of S1 and S2, the most prominent emission originates from the $^5\text{D}_0 \rightarrow ^7\text{F}_2$ transitions, therefore, the Eu^{3+} ions locate at low-symmetry local sites in S1 and S2. Anatase adopts tetragonal symmetry with space group $I4_1/amd$, and the site symmetries for the Ti^{4+} ions are D_{2d} in anatase. According to the branching rules of the 32 point groups, the substitution of the larger Eu^{3+} ions for Ti^{4+} ions creates oxygen vacancies and lattice distortions in the TiO_2 host and makes the site symmetry of the Eu^{3+} ions deviate from the exact D_{2d} symmetry to lower site symmetry. Eu^{3+} symmetry could be defined by asymmetric ratio (A_{21}) of the integrated intensities of $^5\text{D}_0 \rightarrow ^7\text{F}_2$ to $^5\text{D}_0 \rightarrow ^7\text{F}_1$ and A_{21} is calculated to be 3.27 for S1 and 3.23 for S2, respectively, which is attributed to that Eu^{3+} ions in S1 are doped much

more effectively than Eu^{3+} ions in S2 (As XRD results has proved).

Herein, it should be noted that the morphologies of the obtained samples have an important effect on their luminescent intensity, on the premise that the two samples have the same concentration of europium ions. As Figure 9 presented, the PL intensity of the solid microspheres is higher than that of the core-shell ones, which might due to the fewer defects and much more effectively doping of Eu^{3+} ions in the solid microspheres. It is well known that defects of the phosphor crystal provide non-radiative recombination routes for electrons and holes and lead to the luminescence quenching^{37, 38}. It can be speculated that the surface areas of the rough core-shell microspheres are higher than that of the solid microspheres. A large surface area usually introduces a large number of defects into the phosphor crystal³⁹. As a result, the PL intensity of the solid microspheres is higher than that of the core-shell microspheres. On the other hand, Eu^{3+} ions in S1 are doped much more effectively than Eu^{3+} ions in S2, which also results in the the PL intensity of the solid microspheres is higher than that of the core-shell ones.

4. Conclusions

In summary, anatase $\text{TiO}_2:\text{Eu}^{3+}$ microspheres have been successfully prepared by a facile one-step hydrothermal synthesis method. The microspheres can be easily tuned from solid to core-shell structure by the amount of solvent ethanol. Furthermore, the shell and core size of the core-shell microspheres can be controlled by the hydrothermal time through the Ostwald ripening process. The possible formation mechanisms were proposed. In addition, it is also observed that the PL intensity of Eu^{3+} ions depends on the structure of the microspheres. Our work presents a new idea for designing and synthesizing inorganic functional materials.

Acknowledgements

This work is financially supported by the National Natural Science Foundation of China (Grant nos. 21171066 and 51272085), the Opening Research Funds Projects of the State Key Laboratory of Inorganic Synthesis and Preparative (2013-27), and the Key Technology and Equipment of Efficient Utilization of Oil Shale Resources, No. OSR-05.

Figure Captions

Fig. 1 (A) XRD patterns of S1 (a) and S2 (b). The standard data for anatase phase TiO_2 (JCPDS no.21-1272) is also presented for comparison. (B) Local amplification of (101) peaks of S1 (a), S2 (b), and the standard anatase phase TiO_2 (JCPDS no.21-1272).

Fig. 2 EDS spectrum of $\text{TiO}_2:\text{Eu}^{3+}$ solid microspheres (S1).

Fig. 3 XPS spectra of the survey (A), Ti 2p (B), O 1s (C), Eu 3d (D), and Eu 4d (E) for solid $\text{TiO}_2:\text{Eu}^{3+}$ (a) and core-shell $\text{TiO}_2:\text{Eu}^{3+}$ (b).

Fig. 4 SEM (a and b) and TEM (c and d) images of the as-prepared sample S1.

Fig. 5 SEM (a and b) and TEM (c and d) images of the as-prepared sample S2.

Fig. 6 SEM images of the as-prepared samples at different amount of ethanol: (a) 15 mL, (b) 18 mL, (c) 21 mL, (d) 22 mL, (e) 24 mL, and (f) 30 mL.

Fig. 7 SEM images of S2 with different hydrothermal reaction times: (a) 45 min, (b) 90 min, (c) 12 h, (d) 18 h, (e) 4 days, and (f) 6 days.

Fig. 8 Schematic illustration of the formation process of $\text{TiO}_2:\text{Eu}^{3+}$ microspheres.

Fig. 9 PL emission spectra of the (a) solid and (b) core-shell structured $\text{TiO}_2:\text{Eu}^{3+}$ microspheres and the

typical excitation spectrum (inset).

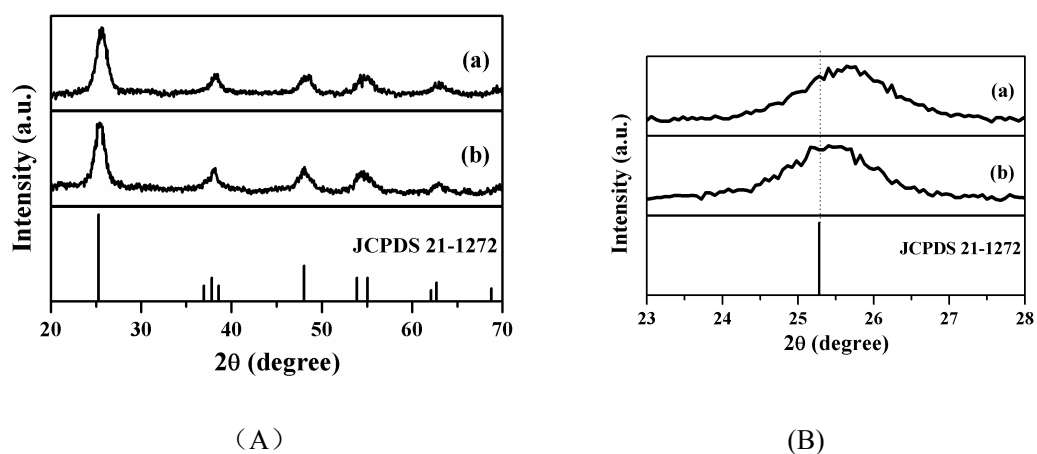


Fig. 1 (A) XRD patterns of S1 (a) and S2 (b). The standard data for anatase phase TiO₂ (JCPDS no.21-1272) is also presented for comparison. (B) Local amplification of (101) peaks of S1 (a), S2 (b), and the standard anatase phase TiO₂ (JCPDS no.21-1272).

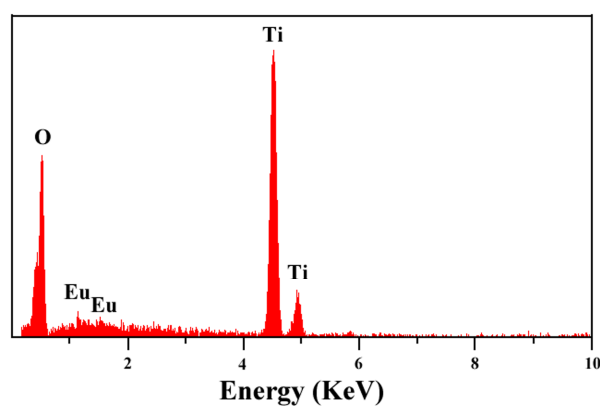


Fig. 2 EDS spectrum of TiO₂:Eu³⁺ solid microspheres (S1).

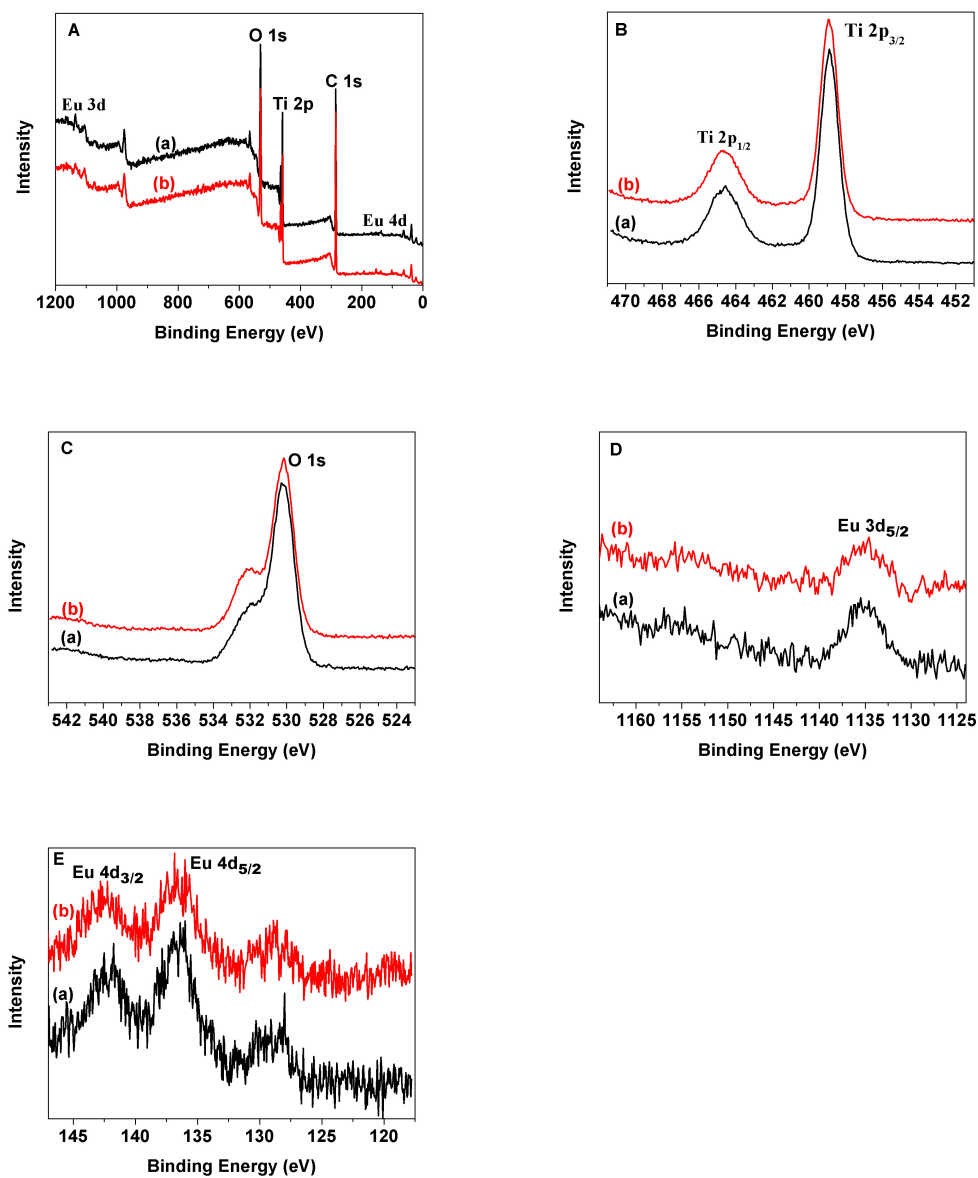


Fig.3 XPS spectra of the survey (A), Ti 2p (B), O 1s (C), Eu 3d (D), and Eu 4d (E) for solid

$\text{TiO}_2:\text{Eu}^{3+}$ (a) and core-shell $\text{TiO}_2:\text{Eu}^{3+}$ (b).

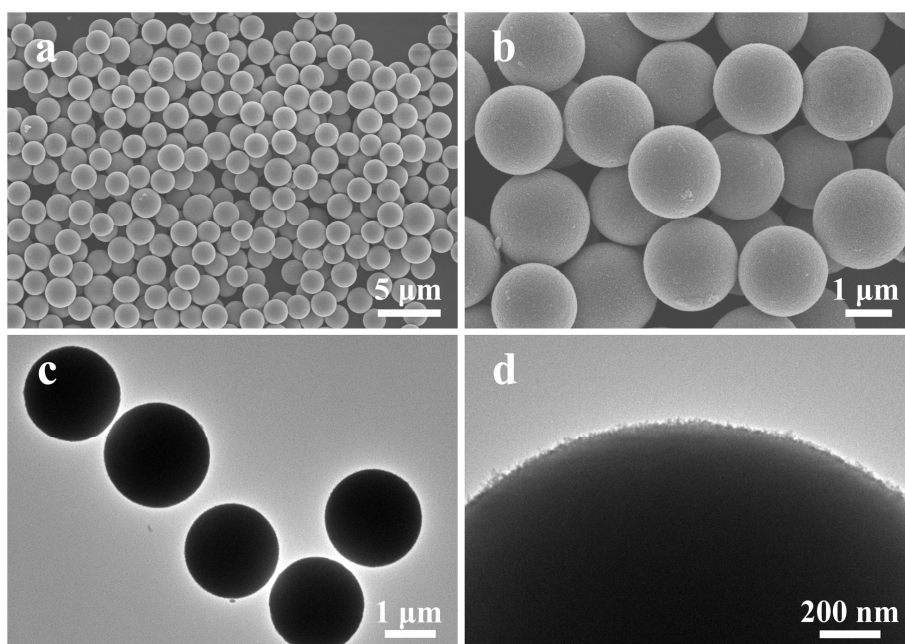


Fig. 4 SEM (a and b) and TEM (c and d) images of the as-prepared sample S1.

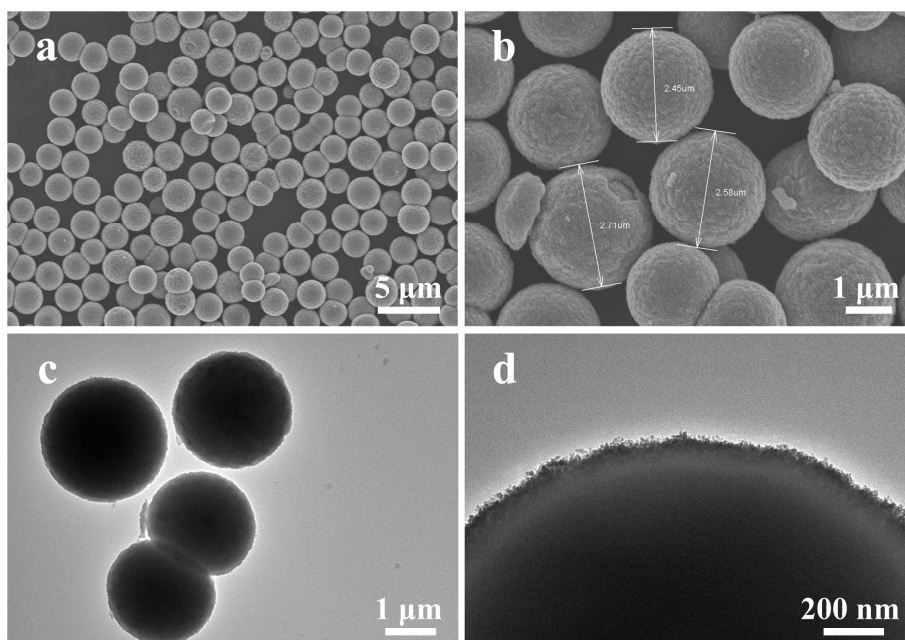


Fig. 5 SEM (a and b) and TEM (c and d) images of the as-prepared sample S2.

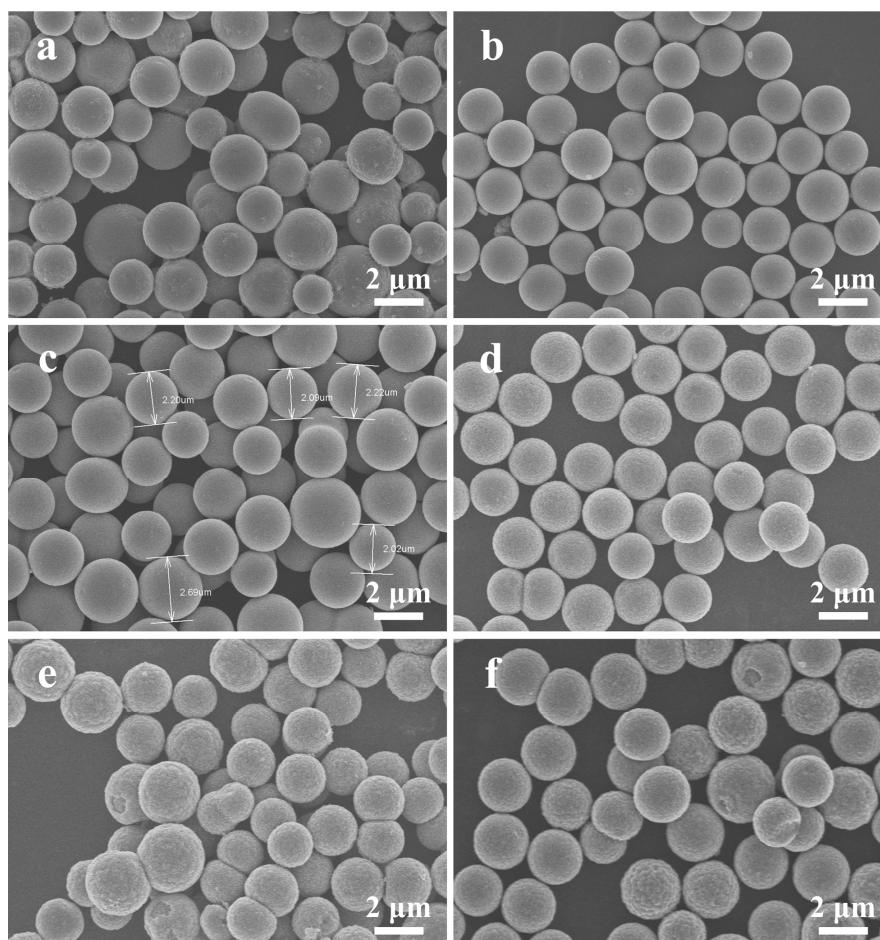


Fig. 6 SEM images of the as-prepared samples at different amount of ethanol: (a) 15 mL, (b) 18 mL, (c) 21 mL, (d) 22 mL, (e) 24 mL, and (f) 30 mL.

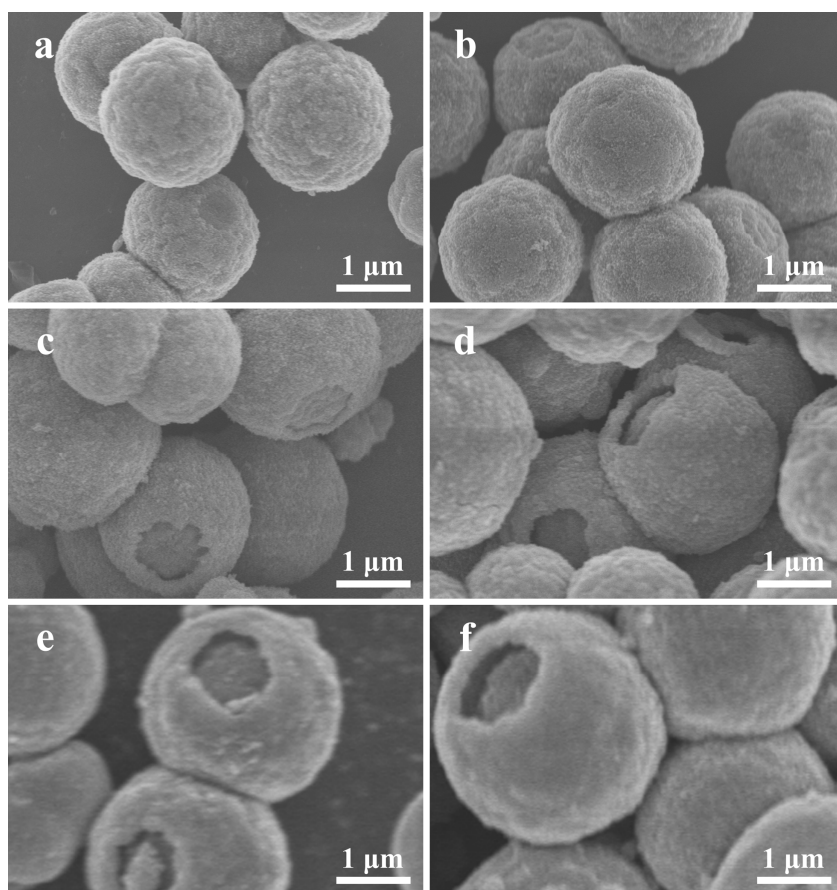


Fig. 7 SEM images of S2 with different hydrothermal reaction times: (a) 45 min, (b) 90 min, (c) 12 h, (d) 18 h, (e) 4 days, and (f) 6 days.

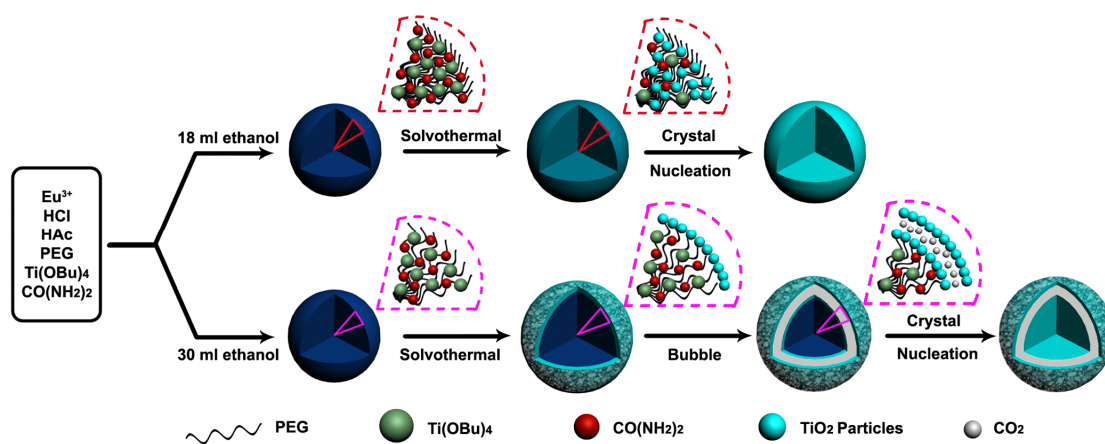


Fig. 8 Schematic illustration of the formation process of $\text{TiO}_2:\text{Eu}^{3+}$ microspheres.

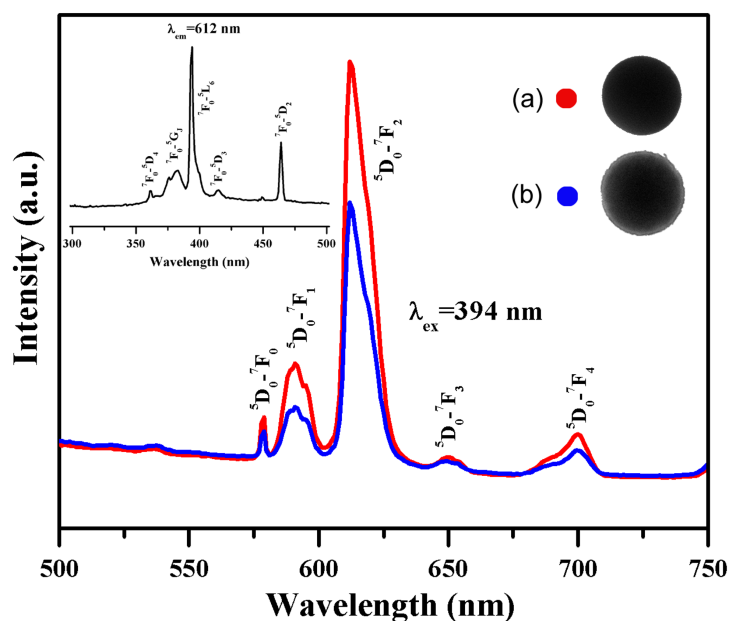


Fig. 9 PL emission spectra of the (a) solid and (b) core-shell structured $\text{TiO}_2:\text{Eu}^{3+}$ microspheres and the typical excitation spectrum (inset).

References

1. Y. Deng, D. Qi, C. Deng, X. Zhang and D. Zhao, *J Am Chem Soc*, 2008, **130**, 28-29.
2. Q. Peng, Y. J. Dong and Y. D. Li, *Angew Chem Int Edit*, 2003, **42**, 3027-3030.
3. V. R. Sinha, A. K. Singla, S. Wadhawan, R. Kaushik, R. Kumria, K. Bansal and S. Dhawan, *Int J Pharm*, 2004, **274**, 1-33.
4. Z. W. Zhang, L. Y. Cao, J. F. Huang, D. Q. Wang, J. P. Wu and Y. J. Cai, *Ceram Int*, 2013, **39**, 2695-2698.
5. S. Dehghanpour, A. Mahmoudi, M. Mirsaeed-Ghazi, N. Bazvand, S. Shadpour and A. Nemati, *Powder Technol*, 2013, **246**, 148-156.
6. R. Razali, A. K. Zak, W. H. Abd Majid and M. Darroudi, *Ceram Int*, 2011, **37**, 3657-3663.
7. Z. Q. Sun, J. H. Kim, Y. Zhao, F. Bijarbooneh, V. Malgras, Y. Lee, Y. M. Kang and S. X. Dou, *J Am Chem Soc*, 2011, **133**, 19314-19317.
8. A. R. Tao, S. Habas and P. D. Yang, *Small*, 2008, **4**, 310-325.
9. T. K. Sau and A. L. Rogach, *Adv Mater*, 2010, **22**, 1781-1804.
10. J. B. Yin, L. Q. Xiang and X. P. Zhao, *Appl Phys Lett*, 2007, **90**, 113112(1-3).
11. W. Q. Luo, R. F. Li, G. K. Liu, M. R. Antonio and X. Y. Chen, *J Phys Chem C*, 2008, **112**, 10370-10377.
12. S. Sandoval, J. Yang, J. G. Alfaro, A. Liberman, M. Makale, C. E. Chiang, I. K. Schuller, A. C. Kummel and W. C. Trogler, *Chem Mater*, 2012, **24**, 4222-4230.
13. H. Hafez, J. Wu, Z. Lan, Q. Li, G. Xie, J. Lin, M. Huang, Y. Huang and M. Abdel-Mottaleb, *Nanotechnology*, 2010, **21**, 415201(6pp).
14. P. Haro-González, M. Pedroni, F. Piccinelli, L. Martín, S. Polizzi, M. Giarola, G. Mariotto, A. Speghini, M. Bettinelli and I. Martín, *Journal of Luminescence*, 2011, **131**, 2473-2477.

15. J. Yin and X. Zhao, *Mater Chem Phys*, 2009, **114**, 561-568.
16. D. K. Yi and D.-Y. Kim, *Nano Lett*, 2003, **3**, 207-211.
17. F. Wang, J. Jiu, L. Pei, K. Nakagawa, S. Isoda and M. Adachi, *Materials Letters*, 2007, **61**, 488-490.
18. L. Li, C. K. Tsung, Z. Yang, G. D. Stucky, L. D. Sun, J. F. Wang and C. H. Yan, *Adv Mater*, 2008, **20**, 903-908.
19. Y. Tian, J. Zhang, J. C. Ma and X. Jia, *Journal of colloid and interface science*, 2012, **385**, 1-7.
20. J. Feng, Y. Hong, J. Zhang, P. Wang, Z. Hu, Q. Wang, L. Han and Y. Zhu, *J Mater Chem A*, 2014, **2**, 1502-1508.
21. G. An, C. Yang, S. Jin, G. Chen and X. Zhao, *J Mater Sci*, 2013, **48**, 5483-5488.
22. Y. Cui, L. Liu, B. Li, X. Zhou and N. Xu, *The Journal of Physical Chemistry C*, 2010, **114**, 2434-2439.
23. H. G. Yang and H. C. Zeng, *The Journal of Physical Chemistry B*, 2004, **108**, 3492-3495.
24. H. Li, Z. Bian, J. Zhu, D. Zhang, G. Li, Y. Huo, H. Li and Y. Lu, *J Am Chem Soc*, 2007, **129**, 8406-8407.
25. H. Li, Y. Sheng, H. Zhang, J. Xue, K. Zheng, Q. Huo and H. Zou, *Powder Technol*, 2011, **212**, 372-377.
26. D. Q. Chen and Y. S. Wang, *Nanoscale*, 2013, **5**, 4621-4637.
27. S. Watanabe, X. L. Ma and C. S. Song, *J Phys Chem C*, 2009, **113**, 14249-14257.
28. S. P. Chenakin, G. Melaet, R. Szukiewicz and N. Kruse, *J Catal*, 2014, **312**, 1-11.
29. N. Kruse and S. Chenakin, *Appl Catal a-Gen*, 2011, **391**, 367-376.
30. F. Mercier, C. Alliot, L. Bion, N. Thromat and P. Toulhoat, *J Electron Spectrosc*, 2006, **150**, 21-26.
31. W.-D. Schneider, C. Laubschat, I. Nowik and G. Kaindl, *Physical Review B*, 1981, **24**, 5422-5425.
32. X. L. Tan, Q. H. Fan, X. K. Wang and B. Grambow, *Environ Sci Technol*, 2009, **43**, 3115-3121.
33. X. Zhou, S. Chen, D. Zhang, X. Guo, W. Ding and Y. Chen, *Langmuir : the ACS journal of surfaces and colloids*, 2006, **22**, 1383-1387.
34. X. Zhou, D. Zhang, Y. Zhu, Y. Shen, X. Guo, W. Ding and Y. Chen, *The Journal of Physical Chemistry B*, 2006, **110**, 25734-25739.
35. Y. Y. Hui and C. F. Lin, *Mater Lett*, 2007, **61**, 3802-3804.
36. Y. H. Zheng, H. P. You, G. Jia, K. Liu, Y. H. Song, M. Yang and H. J. Zhang, *Cryst Growth Des*, 2009, **9**, 5101-5107.
37. Q. Zhao, N. Guo, Y. C. Jia, W. Z. Lv, B. Q. Shao, M. M. Jiao and H. P. You, *J Colloid Interf Sci*, 2013, **394**, 216-222.
38. B. L. Abrams and P. H. Holloway, *Chem Rev*, 2004, **104**, 5783-5801.
39. Q. Zhao, Y. Zheng, N. Guo, Y. Jia, H. Qiao, W. Lv and H. You, *CrystEngComm*, 2012, **14**, 6659-6664.